Copper diffusion into single-crystalline TiN studied by transmission electron microscopy and atom probe tomography

Marlene Muehlbacher, F. Mendez-Martin, B. Sartory, N. Schalk, J. Keckes, Jun Lu, Lars Hultman and C. Mitterer

Linköping University Post Print

N.B.: When citing this work, cite the original article.

Original Publication:

Marlene Muehlbacher, F. Mendez-Martin, B. Sartory, N. Schalk, J. Keckes, Jun Lu, Lars Hultman and C. Mitterer, Copper diffusion into single-crystalline TiN studied by transmission electron microscopy and atom probe tomography, 2015, Thin Solid Films, (574), 103-109.
http://dx.doi.org/10.1016/j.tsf.2014.11.084
Copyright: Elsevier
http://www.elsevier.com/

Postprint available at: Linköping University Electronic Press
http://urn.kb.se/resolve?urn=urn:nbn:se:liu:diva-114436

Copper diffusion into single-crystalline TiN studied by transmission electron microscopy and atom probe tomography

M. Mühlbacher[1,2,*], F. Mendez-Martin[1], B. Sartory[3], N. Schalk[1], J. Keckes[4], J. Lu[2], L. Hultman[2], C. Mitterer[1]

[1] Department of Physical Metallurgy and Materials Testing, Montanuniversität Leoben, Franz-Josef-Strasse 18, A-8700 Leoben, Austria

[2] Thin Film Physics Division, Department of Physics, Chemistry and Biology (IFM), Linköping University, S-581 83 Linköping, Sweden

[3] Materials Center Leoben Forschung GmbH, Roseggerstrasse 12, A-8700 Leoben, Austria

[4] Department of Materials Physics, Montanuniversität Leoben and Erich Schmid Institute for Materials Science, Austrian Academy of Sciences, A-8700 Leoben, Austria

* Corresponding author:
E-mail: marlene.muehlbacher@unileoben.ac.at
Phone: +43 3842 402 4227
+46 1328 8962

Abstract

TiN/Cu bilayers were grown by unbalanced DC magnetron sputter deposition on (001)-oriented MgO substrates. Pole figures and electron back-scatter diffraction orientation maps indicate that both layers in the as-deposited state are single-crystalline with a cube-on-cube epitaxial relationship with the substrate. This is confirmed by selected area electron diffraction patterns. To study the efficiency of the TiN barrier layer against in-diffusion of Cu, samples were annealed at 900 °C for 1 h in vacuum and at 1000 °C for 12 h in Ar atmosphere. The single-crystalline structure of the TiN layer is stable up to annealing temperatures of 1000 °C as shown by high resolution transmission electron microscopy. While no Cu diffusion was evident after annealing at 900 °C, scanning transmission electron microscopy images and energy-dispersive X-ray spectrometry maps show a uniform diffusion layer of about 12 nm after annealing at 1000 °C for 12 h. Concentration depth profiles obtained from 3D atom probe tomography reconstructions confirm these findings and reveal that the TiN film is slightly substoichiometric with a N/Ti ratio of 0.92. Considering this composition, a lattice diffusion mechanism of Cu in TiN via the formation of Cu–N vacancy complexes is proposed. The excellent diffusion barrier properties of single-crystalline TiN are further attributed to the lack of fast diffusion paths such as grain boundaries.

Keywords

TiN, Cu, Diffusion, TEM, APT, Atom probe tomography

1. Introduction

Diffusion barriers are employed in microelectronic devices to prohibit the migration of atoms from the Cu- or Al-based interconnects to adjacent dielectric and semiconductor regions during fabrication and operation. Sputter-deposited TiN barrier layers in Cu metallization schemes have been widely studied because of their high thermal (melting point T_m = 2930 °C) and structural stability combined with a low electrical resistivity (44-197 μΩ cm) [1,2]; thus meeting all the requirements for application in miniaturized electronic devices.

In an early experimental investigation, Chamberlain [3] reported Cu diffusion into r.f. sputtered TiN films with an activation energy E_a = 4.4 eV, which was attributed to grain boundary diffusion. More recent studies have looked into the correlation between the barrier performance and microstructure of TiN films. For example, Moriyama et al. [4] found that polycrystalline TiN films with small mosaic-spread angles and large grain sizes are generally favorable, because the overall amount of grain boundary phase in these films is low. They measured the activation energy for grain boundary and lattice diffusion of Cu to be 1.4 and 2.7 eV, respectively. For nanocrystalline (average grain size around 8 nm) TiN barriers grown by pulsed laser deposition, Gupta et al. [5] observed significantly less Cu diffusion than for comparable polycrystalline and single-crystalline TiN films. An explanation for this behavior could be the effectively much longer diffusion paths along grain boundaries in the case of nano-sized grains. In comparison, columnar grain structures or low angle grain boundaries provide direct diffusion paths in polycrystalline and single-crystalline layers, respectively.

Improved TiN barrier performance was also observed in films with oxidized grain boundaries [6–9]. This mechanism works well for Al metallization by the stuffing of

grain boundaries with Al oxides. However, it is not as effective in Cu metallization because the formation of Cu oxides in the TiN grain boundaries is thermodynamically less favorable [9,10].

While Cu diffusion in TiN barriers has been extensively studied from a phenomenological point of view, especially in the case of lattice diffusion, there is a lack of literature reporting experimental investigations of the underlying atomic migration mechanisms. This may be partly due to the fact that during the early stages of lattice diffusion the diffusion length is so small and the concentration of the diffusing species so low, that it is often below the detection threshold of conventional techniques for chemical analyses. Furthermore, theoretical studies of bulk TiN suggest that point defects present in the TiN barrier layer strongly affect the migration of impurity atoms [11–15]. TiN retains its stable rocksalt structure for a wide stoichiometry range, often resulting in high numbers of native point defects such as vacancies or interstitials that interact with impurity species. For example impurities like O, C, H and Ar can be trapped at N vacancy sites in TiN and may be released again due to interactions with N interstitials. In the cases of C or Ar this results in the formation of stable defect complexes, while O and H are untrapped and released back into the host crystal. This release of O can also explain its segregation to grain boundaries and the subsequent stuffing observed in polycrystalline TiN [15]. Similar interactions with native point defects have been proposed by first-principles calculations for Cu atoms in TiN [12,14].

These point defects are hard to capture accurately by experiment. The two established characterization instruments used today are transmission electron microscopy (TEM) in conjunction with energy-dispersive X-ray spectrometry (EDX) and electron energy loss spectrometry for structural analysis and

compositional/chemical mapping as well as secondary ion mass spectrometry for chemical depth profiling. However, none of these techniques offers true 3D characterization at the atomic scale [16,17].

With the emergence and development of atom probe tomography (APT) in the last decades this gap can now be closed. APT yields a discrete 3D compositional image with very high analytical sensitivity (as good as 1 atom per million) and a spatial resolution of 0.2 - 0.3 nm in all directions. All elements can be detected with an equally high efficiency without prior knowledge of the specimen's composition [16,17]. There are already several reports where APT has been used effectively for the characterization of materials and processes in semiconductor devices and advanced metallization [16,18–20].

The aim of this study is to combine various TEM techniques with APT in order to present a sophisticated and comprehensive analysis approach for the nanometer scale investigation of the interface and inter-diffusion processes in the Cu/bulk TiN system. The present paper shows how the two complementary methods can be used to provide both structural and chemical information of high resolution at buried interfaces. Experimental findings are correlated with results of first-principles studies [11–15]. Ultimately, this information will on the one hand contribute to the understanding of complex segregation and diffusion phenomena; on the other hand this combined experimental approach could become the basis for innovations in materials for microelectronics such as ultrathin and highly effective diffusion and oxidation barrier layers, or - more generally - reliable and degradation-resistant layered materials.

2. Experimental details

TiN/Cu bilayers were grown on (001)-oriented single-crystalline MgO substrates by unbalanced direct current magnetron sputter deposition. Prior to being inserted into the chamber, the MgO wafers were cleaned by successive rinses in ultrasonic baths of acetone and ethanol and blown dry with dry air. The deposition chamber was evacuated to a base pressure below 10^{-5} mbar. Prior to deposition the MgO wafers were etched in an Ar plasma by applying a voltage of -500 V for 5 min to activate and clean the surface. All targets were sputter-cleaned in pure Ar for 5 min as well, with a shutter shielding the substrates.

TiN layers were grown at a substrate temperature of 700 °C in a reactive Ar/N_2 atmosphere (35 sccm Ar, 5 sccm N_2) at a pressure of 4.6×10^{-3} mbar. The power density at the two 2 inch diameter Ti targets was set to 6.2 W cm^{-2} during deposition and an asymmetrically pulsed bias potential of -100 V was applied to the substrates to provide additional energy for the film forming species [21]. This resulted in a deposition rate of 11 nm min^{-1} for TiN. Without breaking the vacuum, the Cu overlayers were grown on the TiN film at a substrate temperature of 50 °C in pure Ar atmosphere. The power density at the single 2 inch diameter Cu target was set to 2.1 W cm^{-2} and the deposition was carried out at floating potential, yielding a growth rate of 13 nm min^{-1}.

Three sets of bilayers with different layer thicknesses as measured in cross-sectional TEM were produced: TiN (160 nm) / Cu (20 nm), TiN (100 nm) / Cu (130 nm), and TiN (80 nm) / Cu (130 nm). The samples with the thicker Cu film were used in the subsequent annealing studies, where Cu acted as the diffusion source. Isothermal annealing treatments were performed in vacuum ($p < 10^{-6}$ mbar) for 1 h at 900 °C, and in Ar atmosphere for 12 h at 1000 °C. The choice of a protective gas

atmosphere for the high temperature annealing treatment was necessary to prohibit Cu evaporation. It has to be noted that during the annealing treatments de-wetting of the Cu layer and consequently Cu island formation was observed. In the following investigations, the Cu diffusion into TiN was studied directly beneath the center of such Cu islands, to ensure that a sufficient amount of diffusing species was available.

Pole figure measurements were performed using a Rigaku SmartLab 5-axis diffractometer equipped with Cu-K_α radiation, a parabolic multilayer mirror in the primary beam and a secondary graphite monochromator in 5° steps for the azimuth angle Ψ, $0° \leq \Psi \leq 85°$, and the polar angle Φ, $0° \leq \Phi \leq 360°$. The data was evaluated using the MATLAB® toolbox MTEX 3.5.0 for quantitative texture analysis [22].

Single-layer TiN films deposited with the same parameters as the bilayer films were used to determine the density and surface roughness of the TiN film by X-ray reflectivity (XRR) measurements and to study the TiN surface by electron back-scatter diffraction (EBSD) and atomic force microscopy (AFM). XRR characterization was performed using the Rigaku system in the same setup as for the pole-figure analysis. For the fitting of the measured data the Leptos Bruker software was used. Values for the density and surface roughness of the TiN layer were obtained by fitting the critical angle and the intensity slope according to the Nevot-Croce interface model with a genetic algorithm fit. EBSD scans were performed with an EDAX DigiView IV EBSD detector inside a scanning electron microscope (SEM). Areas of 10 x 10 μm^2 were scanned with the pixel size set to 30 nm^2. The surface roughness of the as-deposited TiN layer was also measured by AFM in tapping mode in ambient atmosphere with a BRR/SPM device designed by DME.

Elemental composition of the film was obtained by time-of-flight energy elastic recoil detection analysis (ToF-E ERDA). 36 MeV $^{127}I^{8+}$ ions were used as projectiles with the incident angle set to 67.5° with respect to the surface normal and a recoil angle of 45° [23]. The recoil ToF-E ERDA spectra were analyzed using the CONTES code [24], where the measured recoil energy spectrum of each element was converted to relative atomic concentration, providing an error margin of ±1.5 at.% for the reported elemental compositions.

Samples for APT and TEM were prepared using the focused ion beam (FIB) lift-out technique in a Zeiss Auriga SMT SEM equipped with an Orsay Physics Cobra Z-05 FIB unit with a Ga^+ ion source. In a final step all samples were polished with 5 kV Ga^+ ions to remove surface defects. Additional TEM samples were prepared by the conventional method, where specimens glued into a Ti grid are mechanically polished down to a thickness of approximately 60 µm. Etching of the samples was completed in a Gatan precision ion polishing system by bombardment with 5 keV Ar^+ ions until electron transparency was reached. Fine polishing was performed in the same system using 2 keV Ar^+ ions.

High resolution transmission electron microscopy (HRTEM), collection of selected area diffraction (SAED) patterns and scanning transmission electron microscopy (STEM) were carried out by using a FEI Tecnai G^2 TF20 UT TEM with a field emission gun operated at 200 kV. The instrument has a point resolution of 0.19 nm and is equipped with an EDX system. EDX analyses were performed during STEM investigation to obtain elemental composition maps across the interfaces. Furthermore, Z-contrast STEM imaging with a high-angle annular dark field (HAADF) detector was employed to detect electrons elastically scattered from the specimen with high angles, thus providing strong atomic number contrast in the image.

Samples were also analyzed in a local electrode atom probe (Imago LEAP 3000X HR) in laser pulsing mode with a pulse rate of 200 kHz and pulse energy of 0.2 nJ at 60 K. All APT samples had a similar specimen geometry with a tip radius smaller than 50 nm and a shank angle in the range of 10°. Three tips of each sample state (as-deposited, annealed 900 °C for 1 h, annealed 1000 °C for 12 h) were examined. The investigated volume was in the range of 400,000 nm^3. For reconstruction and chemical analysis with the Cameca IVAS 3.6.6 software, an evaporation field of 30 V nm^{-1}, image compression factor of 1.65 and field factor of 3.3 were used. The reconstruction was based on the tip radius evolution with increasing evaporation voltage.

3. Results and discussion

3.1 Structural and compositional characterization

Fig. 1 shows X-ray diffraction (XRD) pole figure maps of a TiN (160 nm thickness) / Cu (20 nm thickness) bilayer grown on MgO(001). The pole figures were measured at constant 2 theta angles corresponding to the (111) and (200) reflections of TiN and Cu. At this point it has to be noted that because of the lattice mismatch of only -0.7% [19,20] between TiN and MgO their reflections nearly overlap. Due to the small film thicknesses, the substrate will partly contribute to the measured TiN pole figures. Nevertheless, in the 002-pole figures of both layers (Figs. 1a, c) there are no maxima present apart from the single one at the origin. This indicates that all (001) planes in the TiN and the Cu film are oriented parallel to the substrate surface. The weak maximum in the center of the Cu 111-pole figure (Fig. 1d) results from the (200) reflection of MgO (and possibly TiN), whose 2 theta angle of 42.917° [25] (TiN: 42.597° [26]) is very close to that of the Cu (111) reflection at 43.298° [27]. On the

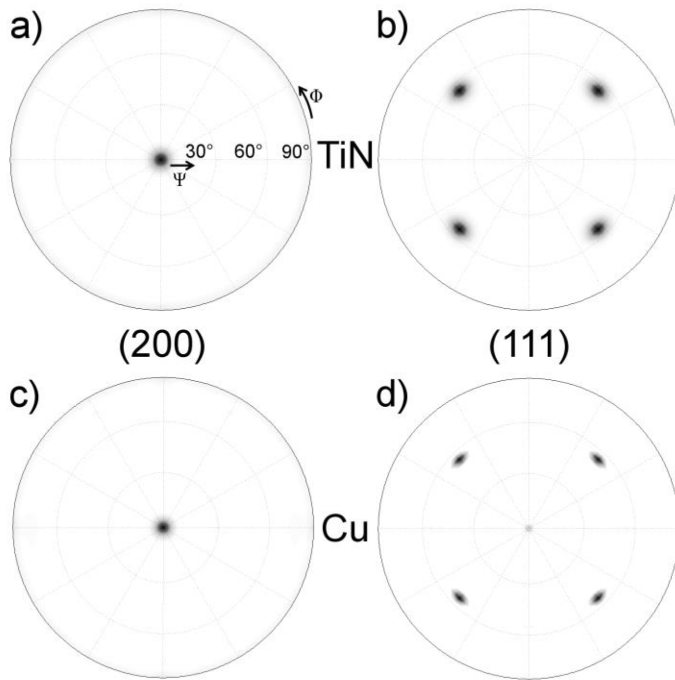

Figure 1: XRD pole figures obtained from the respective (a, c) (200) and (b, d) (111) reflections of TiN (160 nm) / Cu (20 nm) bilayers grown on (001)-oriented MgO substrates.

other hand, in both 111-pole figures (Figs. 1b, d) four symmetric maxima at a tilt angle of about 55° can be observed. In cubic materials the angle between the (001) and (111) planes is 54.7°, again suggesting that TiN/Cu bilayers grow with their (001) planes parallel to the MgO (001) planes. Additionally, the maxima corresponding to the {111} planes of TiN and Cu appear at polar angles of 45, 135, 225 and 315°. Therefore, it can be concluded that the bilayers grow with a cube-on-cube epitaxial relationship on the substrate, i.e. {001}<010>TiN/Cu || {001}<010>MgO.

Fig. 2 shows plan-view EBSD scans of the TiN and Cu surfaces. In the case of TiN some pixels give diffraction information deviating from the expected (001) orientation. These are most likely pixel errors due to debris on the surface and not actual growth defects. Otherwise the misorientation would carry on into the Cu toplayer, which is not the case as can be seen in Fig. 2b. Thus, the EBSD scans

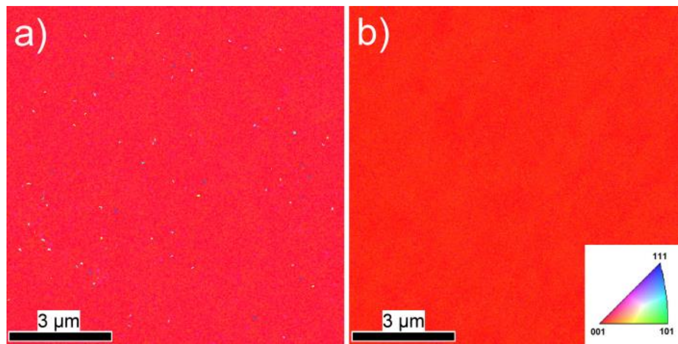

Figure 2: Plan-view EBSD maps of the (a) TiN and (b) Cu surface, recorded over an area of 10 x 10 µm^2 with a pixel size of 30 nm^2. The TiN and Cu layers were 160 and 20 nm thick, respectively.

further point to the epitaxial, single-crystalline growth of fcc TiN/Cu bilayers on (001)-oriented MgO.

The average surface roughness of the TiN layer was measured to be below 0.8 nm by AFM, which is in the range of the surface roughness of the substrate. A fit of the XRR curve of the TiN layer yielded a comparable roughness value of 0.9 ± 0.2 nm.

Cross-sectional samples of the as-deposited and annealed bilayers were investigated by conventional TEM. In both cases the observable region of the TiN layer was free of grain boundaries, indicating that the film is single-crystalline. HRTEM micrographs (Figs. 3a, b) and the corresponding SAED patterns (inserts in Figs. 3a, b) of both the TiN/MgO and Cu/TiN interfaces in the as-deposited state were recorded along the [100] zone axis. In Fig. 3a the (020) lattice spacings of MgO and TiN were both measured to be 0.21 nm. Because of the small lattice mismatch there is an overlap in the SAED patterns, which confirm the epitaxial relationship found by the pole figure maps. No indication of Mg-Ti-spinel formation at the interface, as previously reported in [28], could be detected during the TEM investigations or in the SAED patterns. The measured (020) lattice spacing of 0.18 nm in Cu (Fig. 3b) goes along with clearly discernible reflections in the

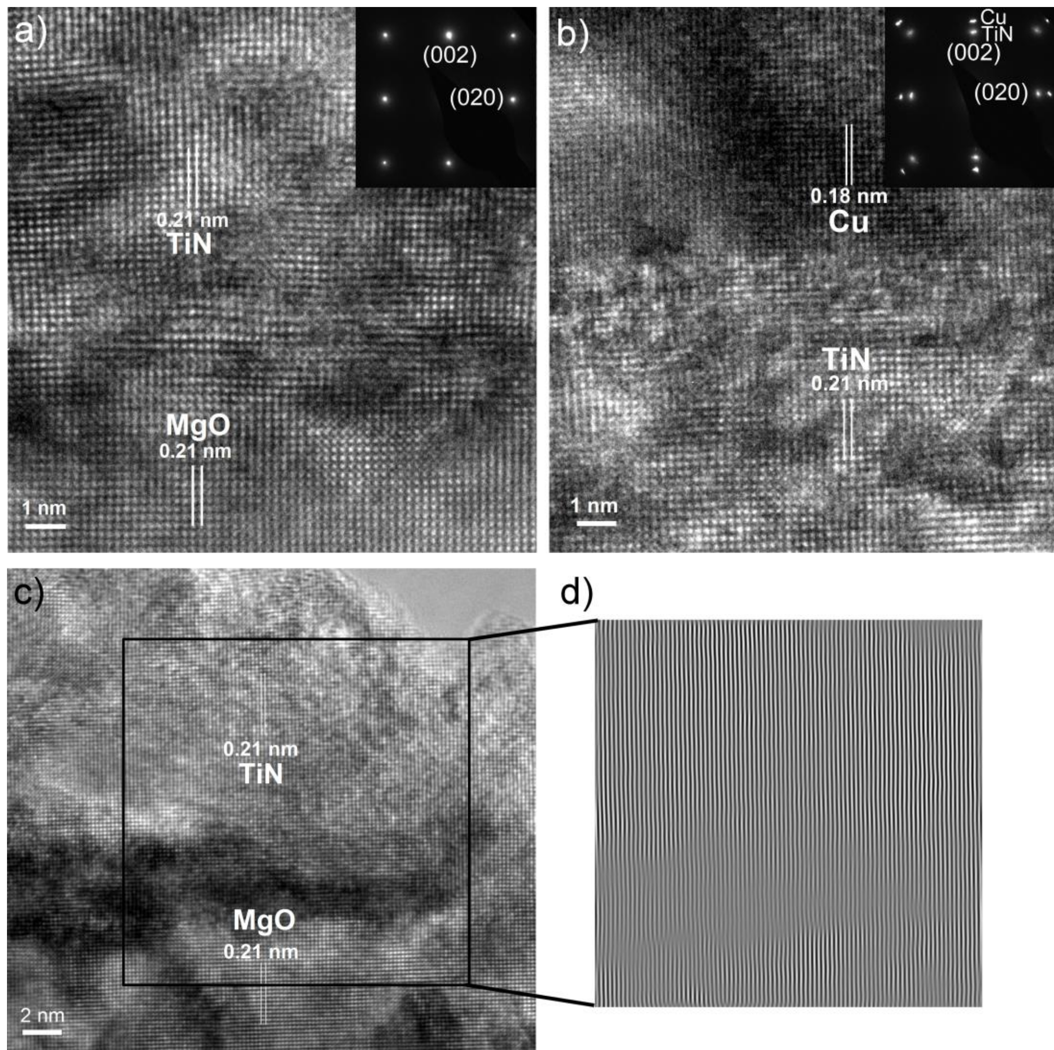

Figure 3: Cross-sectional HRTEM images of the (a) TiN/MgO and (b) Cu/TiN interface in the as-deposited state and corresponding SAED patterns (inserts) recorded along the [100] zone axis. The TiN and Cu layers were 160 and 20 nm thick, respectively. A high resolution micrograph of the TiN/MgO interface after annealing at 1000 °C for 12 h recorded along the [100] zone axis is shown in (c) as well as the corresponding calculated (020) Bragg image in (d).

corresponding SAED pattern of the Cu/TiN interface, again confirming epitaxial, single-crystalline film growth.

Fig. 3c shows a HRTEM micrograph of the TiN/MgO interface after annealing for 12 h at 1000 °C in Ar atmosphere. The TiN layer remains stable up to this temperature and no reaction with the MgO substrate was observed. Since there is a considerable difference in the thermal expansion coefficients of TiN and MgO, the compressive stress due to differential thermal contraction after cooling down the

sample from the deposition temperature of 700 °C is calculated to be 2.2 GPa in the TiN film [29]. It can be assumed that at least a part of that stress is relieved by the formation of dislocations. Thus, annealing the film above the deposition temperature again will lead to a significant decrease in dislocation density. This is corroborated by the (020) Bragg image of the annealed TiN layer (Fig. 3d), where no dislocations could be found in the layer. However, there are some misfit dislocations present directly at the interface, which is revealed by a darker contrast in the Bragg image. Overall, the low dislocation density and the lack of direct diffusion paths such as grain boundaries potentially enhance the performance of the single-crystalline TiN diffusion barrier.

3.2 Diffusion studies

3.2.1 Experimental findings

The diffusion depth of Cu in the annealed samples was evaluated by STEM Z-contrast imaging techniques [30] and EDX mappings. After annealing at 900 °C for 1 h in vacuum, no perceptible Cu diffusion into bulk TiN was detected. A STEM image obtained with a HAADF detector is shown in Figs. 4a, b. Cu as the heaviest element gives the brightest contrast while MgO appears darkest. Figs. 4c, d show EDX mappings of the Cu-K and the Ti-K edge recorded across the Cu/TiN interface with the pixel size set to 1 nm^2. In both the STEM image and the EDX mappings, the Cu/TiN interface appears sharp and well defined in terms of elemental distribution and no indications of Cu diffusion could be found over the investigated area.

Results for the sample annealed at 1000 °C for 12 h in Ar atmosphere are shown in Figs. 4e-h. The STEM Z-contrast image (Figs. 4e, f) reveals a layer with lighter contrast reaching from the Cu/TiN interface into the TiN film. EDX mappings

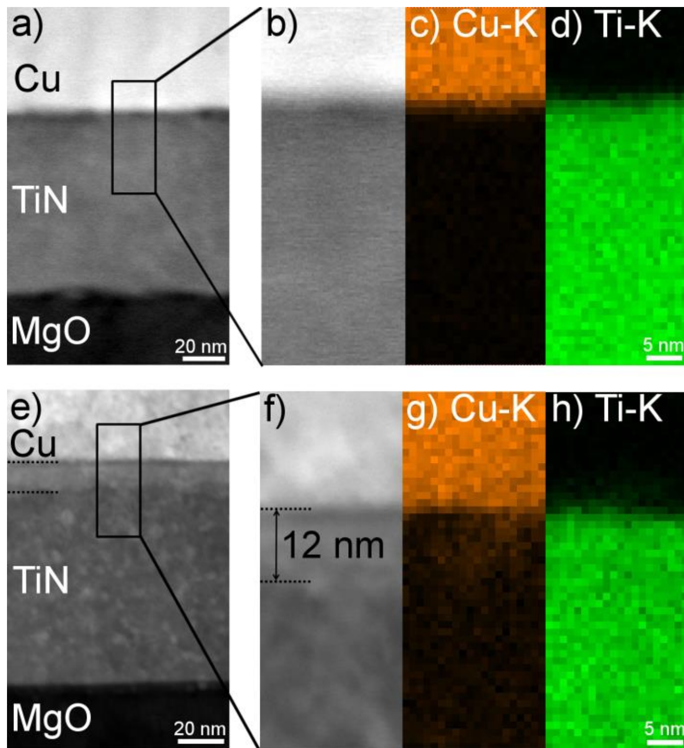

Figure 4: Cross-sectional STEM images obtained with a HAADF detector of samples with an initial Cu layer thickness of 130 nm annealed at (a, b) 900 °C for 1 h and at (e, f) 1000 °C for 12 h. The zoom denotes the areas where EDX maps of the (c) Cu-K and (d) Ti-K edge for the 900 °C sample and of the (g) Cu- K and (h) Ti-K edge for the 1000 °C sample have been recorded. The diffusion layer after annealing at 1000 °C is marked in (e, f).

(Figs. 4g, h) suggest that this layer is due to Cu diffusion into the bulk TiN. While the interface appears relatively sharp when mapping the Ti-K edge (Fig. 4h), mapping of the Cu-K edge (Fig. 4g) shows diffused Cu in the single-crystalline TiN film. The uniformity of the diffusion layer indicates that Cu diffuses via a bulk diffusion mechanism. Based upon the contrast difference in the STEM image the diffusion length was measured to be approximately 12 nm.

The characteristic diffusion length $\bar{x}$ is given by

$$\bar{x} = 2 * \sqrt{Dt} \quad , \qquad (1)$$

where D is the diffusion coefficient at a given temperature and t the time for diffusion. With the measured diffusion length of 12 nm, the diffusion coefficient at 1000 °C can thus be calculated to be about 8×10^{-18} $cm^2 s^{-1}$. In comparison, diffusion coefficients published for polycrystalline TiN barrier layers are typically in the range of

10^{-15} - 10^{-14} cm^2s^{-1} for annealing temperatures of 900 °C and would be even higher at 1000 °C [4,31]. This illustrates the strong influence of grain boundaries on the performance of the diffusion barrier.

To support the TEM investigations, concentration depth profiles were extracted from APT reconstructions of the Cu/TiN interface of the pristine and annealed samples as shown in Fig. 5. Due to its high sensitivity and sub-nanometer resolution, APT can provide detailed insights into the elemental distribution directly at the interface. APT reveals that the TiN film is slightly substoichiometric for all three sample states (Fig. 5a). In the case of the annealed samples there seems to be a further N loss directly at the interface, but from a depth of about 5 nm into the TiN film, the composition of all three sample states is identical.

A quantitative comparison of the elemental composition of the as-deposited TiN layer as measured by ERDA and APT is given in Tab. 1. The results of the two analyses are in excellent agreement, especially regarding the stoichiometry of the TiN film. Both techniques give a N/Ti ratio of 0.92, indicating the presence of N vacancies in the TiN layer. The measurement error of ERDA is below 1.5 at.% and of APT below 0.1 at.% for all analyzed elements. Deviations in the measured Ar and O contents are present at the error margin of ERDA.

Table 1: Comparison of the elemental composition of the as-deposited TiN film measured by ERDA and APT.

	Ti [at.%]	N [at.%]	Ar [at.%]	O [at.%]	C [at.%]
ERDA	50.9	47.0	1.6	0.1	0.4
APT	51.0	47.2	0.9	0.8	0.1

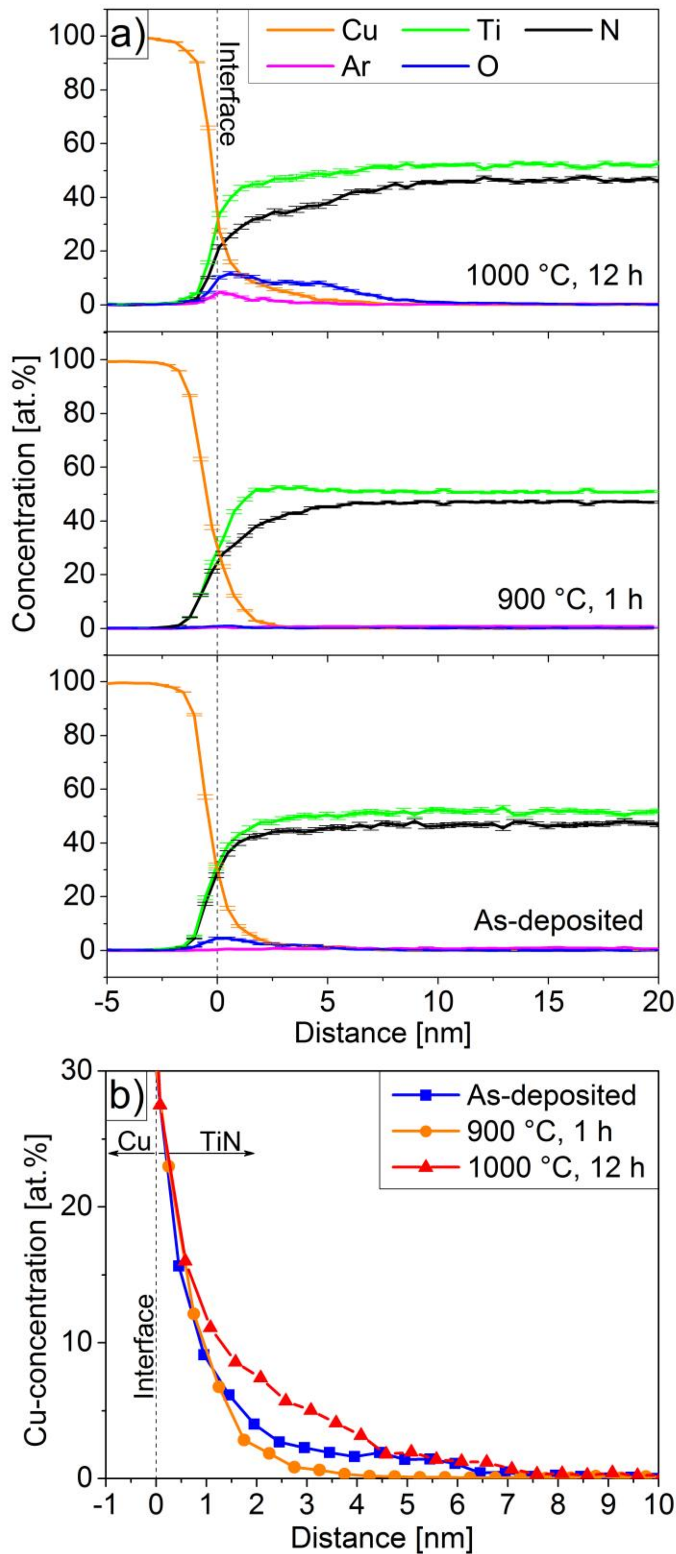

Figure 5: Concentration depth profiles with error bars acquired from representative 3D APT reconstructions of all three sample states (a) and a comparison of the Cu distribution directly at the interface (b). The initial Cu layer thickness was 20 nm in case of the pristine sample and 130 nm in case of the annealed sample states.

In order to test the finding of a slight substoichiometry of the TiN films, XRR measurements of single-layer TiN were performed. The results show a density of 5.4 ± 0.2 g cm^{-3}, which is in agreement with the bulk value of 5.39 g cm^{-3} [32]. Since the TiN density is a direct function of the N concentration in TiN_x ($0.6 \leq x \leq 1.2$) [33], we conclude that the TiN films are at most slightly substoichiometric. Also the films are effectively dense without porosity or open percolation paths, as supported by the TEM analyses (Figs. 3 and 4).

The evident Ar incorporation into TiN is a side effect of the biased sputtering process in mixed N_2-Ar atmosphere. According to Hultman et al. [34], Ar will likely be incorporated interstitially or in the form of small bubbles (< 2 nm). Furthermore, an O enrichment directly at the Cu/TiN interface is observable in the as-deposited sample in Fig. 5a, although no indications for this could be found during the TEM investigations. This O accumulation can most likely be related to the cooling process between the TiN and Cu depositions, where residual gas in the chamber could have adsorbed on the TiN surface. However, the fact that the Cu overlayer adopts the (001) orientation of the underlying TiN points towards a negligibly thin adsorbate layer, so that it could not be resolved with HRTEM. The O enrichment at the interface is not discernible after the 900 °C annealing treatment in vacuum. Presumably the low amounts of O have diffused into the Cu and TiN layers during the annealing treatment, where they are now evenly distributed as impurities. In case of the sample annealed at 1000 °C in Ar atmosphere, again higher levels of Ar and O are present at the Cu/TiN interface, which is probably a side effect of the annealing treatment and the aforementioned Cu island formation. It is conceivable that during this process Ar and residual O are captured at the interface of the formed Cu islands and the underlying TiN film. The following considerations will not take into account

the influence of the O and Ar impurities that were found by APT on the Cu bulk diffusion. Especially in transition metal nitrides, the interplay of defects and impurities is very complex and its comprehensive analysis would go beyond the scope of this study. As shown in Fig. 5a the Cu/TiN interface is spread over approximately 2 nm in the as-deposited sample. From the direct comparison of the Cu depth concentration profiles in Fig. 5b no significant change in the Cu distribution is evident after annealing at 900 °C for 1 h. This is in agreement with the findings of STEM and EDX mapping. On the other hand, after annealing at 1000 °C for 12 h first indications of beginning Cu diffusion are evident in Fig. 5b. A slightly elevated Cu concentration is apparent, reaching from the interface approximately 7 nm into the TiN layer. This diffusion length agrees reasonably well with the 12 nm measured in the STEM image. This is an exceptionally short diffusion length compared to values published for polycrystalline TiN diffusion barriers [4,5,35]. A possible reason for the higher efficiency of single-crystalline TiN barrier layers is the absence of fast diffusion paths in the form of grain boundaries. The diffusion mechanism is solely controlled by lattice diffusion, where the activation energy is much higher.

3.2.2 Relation to theoretical studies

Extensive theoretical studies illustrating diffusion of Cu and other species in TiN are available by Tsetseris et al. [11–15], where especially the importance of the defect structure in the TiN film is analyzed based on density-functional theory. In a perfectly stoichiometric, defect-free TiN film the activation energy E_a for diffusion of an interstitial Cu atom was calculated to be 1.4 eV. However, if there is a small number of N vacancies present in the TiN, the Cu atom may be trapped at a N vacancy site with a binding energy of 4.08 eV. According to Tsetseris et al. the migration

activation energy for such a trapped Cu atom would be so large that in fact it can be considered immobile. A different mechanism emerges when the density of N vacancies becomes so high that another N vacancy is in the vicinity of the trapped Cu atom. The Cu atom can now move to the neighboring N vacancy site while leaving behind a new vacancy. In a second step this new vacancy will then hop to a vicinal N site. The effective activation energy for the migration of such a complex is 2.8 eV [12,14].

Considering the composition of the TiN layers investigated in the present study (Tab. 1), the formation and migration of Cu-N vacancy complexes should be the energetically most favorable atomic-scale mechanism for the lattice diffusion of Cu atoms. With the diffusion coefficient D = 8×10^{-18} cm^2s^{-1} calculated from the measured diffusion length after annealing at 1000 °C, the pre-exponential factor D_0 can be obtained from the Arrhenius-relation

$$D = D_0 * \exp\left(-\frac{E_a}{kT}\right) , \quad (2)$$

where k denotes the Boltzmann constant and T is the absolute temperature. Solving this equation yields a pre-exponential factor $D_0 = 9.7 \times 10^{-7}$ cm^2s^{-1}.

In summary, Cu diffusion is not active in substoichiometric bulk TiN when Cu atoms get trapped at isolated N vacancies and moderate when the Cu atom can diffuse as a complex together with a N vacancy. If no grain boundaries or fast percolation paths such as connected N vacancy networks are present, the migration of Cu atoms is controlled by a lattice diffusion mechanism.

4. Conclusions

A complementary combination of HRTEM, STEM and APT was established to study the bulk diffusion of Cu in TiN. HRTEM confirmed the single-crystalline structure of

the TiN layer, and APT uncovered low levels of O and Ar impurities at the interface and revealed a substoichiometry of the TiN film. No discernible Cu diffusion was observed with either technique after annealing at 900 °C for 1 h. After an annealing treatment at 1000 °C for 12 h, a uniform inter-diffusion layer with a thickness of 12 nm was observable in STEM images, indicating that Cu diffused via a lattice diffusion mechanism in single-crystalline TiN. APT depth concentration profiles showed a comparable diffusion length of 7 nm.

With these values the diffusion coefficient at 1000 °C was calculated to be about 8×10^{-18} cm^{2}s^{-1}. A comparison to theoretical studies [11–15] based on density-functional theory shows that the likely diffusion mechanism in the present substoichiometric TiN films is Cu migration from one N vacancy site to another with an activation energy of 2.8 eV and a pre-exponential factor of about 9.7×10^{-7} cm^{2}s^{-1}. The lack of fast diffusion paths such as grain boundaries contributes to the excellent diffusion barrier properties of single-crystalline TiN.

5. Acknowledgements

The authors are grateful to Jens Jensen (Thin Film Physics Division, IFM, Linköping University, Sweden) for the execution, evaluation and discussion of ERDA and to Juraj Todt (Erich Schmid Institute for Materials Science, Austrian Academy of Sciences) for pole figure measurements and the fruitful input regarding their analysis as well as to Livia Chitu (Materials Center Leoben Forschung GmbH, Austria) for AFM and XRR measurements. Furthermore, Elisabeth Jäger and Katharina Taferner (both Materials Center Leoben Forschung GmbH, Austria) are acknowledged for experimental work.

Financial support by the Austrian Federal Government (in particular from Bundesministerium für Verkehr, Innovation und Technologie and Bundesministerium für Wirtschaft, Familie und Jugend) represented by Österreichische Forschungsförderungsgesellschaft mbH and the Styrian and the Tyrolean Provincial Government, represented by Steirische Wirtschaftsförderungsgesellschaft mbH and Standortagentur Tirol, within the framework of the COMET Funding Programme is gratefully acknowledged.

LH acknowledges support from the Swedish Research Council Project Grant # 2013-4018 and the Knut and Alice Wallenberg Foundation for the Electron Microscopy Laboratory at Linköping University operated by the Thin Film Physics Division.

6. References

[1] K.-C. Park, K.-B. Kim, I.J.M.M. Raaijmakers, K. Ngan, The effect of density and microstructure on the performance of TiN barrier films in Cu metallization, J. Appl. Phys. 80 (1996) 5674–5681.

[2] S.-Q. Wang, I. Raaijmakers, B.J. Burrow, S. Suthar, S. Redkar, K.-B. Kim, Reactively sputtered TiN as a diffusion barrier between Cu and Si, J. Appl. Phys. 68 (1990) 5176–5187.

[3] M.B. Chamberlain, Diffusion of copper in thin TiN films, Thin Solid Films. 91 (1982) 155–162.

[4] M. Moriyama, T. Kawazoe, M. Tanaka, M. Murakami, Correlation between microstructure and barrier properties of TiN thin films used Cu interconnects, Thin Solid Films. 416 (2002) 136–144.

[5] A. Gupta, H. Wang, A. Kvit, G. Duscher, J. Narayan, Effect of microstructure on diffusion of copper in TiN films, J. Appl. Phys. 93 (2003) 5210–5214.

[6] M. Mändl, H. Hoffmann, P. Kücher, Diffusion barrier properties of Ti/TiN investigated by transmission electron microscopy, J. Appl. Phys. 68 (1990) 2127–2132.

[7] W. Sinke, G.P.A. Frijlink, F.W. Saris, Oxygen in titanium nitride diffusion barriers, Appl. Phys. Lett. 47 (1985) 471–473.

[8] J.O. Olowolafe, J. Li, J.W. Mayer, E.G. Colgan, Effects of oxygen in TiN_x on the diffusion of Cu in Cu/TiN/Al and Cu/TiN_x/Si structures, Appl. Phys. Lett. 58 (1991) 469–471.

[9] K.T. Nam, A. Datta, S.-H. Kim, K.-B. Kim, Improved diffusion barrier by stuffing the grain boundaries of TiN with a thin Al interlayer for Cu metallization, Appl. Phys. Lett. 79 (2001) 2549–2551.

[10] K.-C. Park, K.-B. Kim, Effect of Annealing of Titanium Nitride on the Diffusion Barrier Property in Cu Metallization, J. Electrochem. Soc. 142 (1995) 3109–3115.

[11] L. Tsetseris, N. Kalfagiannis, S. Logothetidis, S.T. Pantelides, Structure and interaction of point defects in transition-metal nitrides, Phys. Rev. B. 76 (2007) 2241071–2241077.

[12] L. Tsetseris, S. Logothetidis, S.T. Pantelides, Atomic-scale mechanisms for diffusion of impurities in transition-metal nitrides, Surf. Coat. Technol. 204 (2010) 2089–2094.

[13] L. Tsetseris, N. Kalfagiannis, S. Logothetidis, S.T. Pantelides, Role of N defects on thermally induced atomic-scale structural changes in transition-metal nitrides, Phys. Rev. Lett. 99 (2007) 1255031–1255034.

[14] L. Tsetseris, S. Logothetidis, S.T. Pantelides, Migration of species in a prototype diffusion barrier: Cu, O, and H in TiN, Appl. Phys. Lett. 94 (2009) 1619031–1619033.

[15] L. Tsetseris, N. Kalfagiannis, S. Logothetidis, S.T. Pantelides, Trapping and release of impurities in TiN: A first-principles study, Phys. Rev. B. 78 (2008) 0941111–0941119.

[16] T.F. Kelly, D.J. Larson, K. Thompson, R.L. Alvis, J.H. Bunton, J.D. Olson, B.P. Gorman, Atom probe tomography of electronic materials, Annu. Rev. Mater. Res. 37 (2007) 681–727.

[17] T.F. Kelly, M.K. Miller, K. Rajan, S.P. Ringer, Atomic-scale tomography: A 2020 vision, Microsc. Microanal. 19 (2013) 652–664.

[18] D. Mangelinck, F. Panciera, K. Hoummada, M. El Kousseifi, C. Perrin, M. Descoins, A. Portavoce, Atom probe tomography for advanced metallization, Microelectron. Eng. 120 (2014) 19–33.

[19] E.A. Marquis, M. Bachhav, Y. Chen, Y. Dong, L.M. Gordon, A. McFarland, On the current role of atom probe tomography in materials characterization and materials science, Curr. Opin. Solid State Mater. 17 (2013) 217–223.

[20] F. Panciera, K. Hoummada, M. Gregoire, M. Juhel, F. Lorut, N. Bicais, D. Mangelinck, Atom probe tomography of SRAM transistors: Specimen preparation methods and analysis, Microelectron. Eng. 107 (2013) 167–172.

[21] N. Jiang, H.J. Zhang, S.N. Bao, Y.G. Shen, Z.F. Zhou, XPS study for reactively sputtered titanium nitride thin films deposited under different substrate bias, Phys. B Condens. Matter. 352 (2004) 118–126.

[22] F. Bachmann, R. Hielscher, H. Schaeben, Texture analysis with MTEX – Free and open source software toolbox, Solid State Phenom. 160 (2010) 63–68.

[23] J. Jensen, D. Martin, A. Surpi, T. Kubart, ERD analysis and modification of TiO_2 thin films with heavy ions, Nucl. Inst. Methods B. 268 (2010) 1893–1898.

[24] M.S. Janson, CONTES, Conversion of time-energy spectra, a program for ERDA data analysis, Internal Report, Uppsala University, 2004.

[25] Powder Diffraction File 00-045-0946, International Center for Diffraction Data, PDF-2/Release, 2007.

[26] Powder Diffraction File 00-038-1420, International Center for Diffraction Data, PDF-2/Release, 2007.

[27] Powder Diffraction File 00-004-0836, International Center for Diffraction Data, PDF-2/Release, 2007.

[28] L. Hultman, Thermal stability of nitride thin films, Vacuum. 57 (2000) 1–30.

[29] G. Abadias, Y.Y. Tse, Determination of intrinsic stresses in textured and epitaxial TiN thin films deposited by dual ion beam sputtering, Surf. Coat. Technol. 180-181 (2004) 33–40.

[30] H. Wang, A. Tiwari, X. Zhang, A. Kvit, J. Narayan, Copper diffusion characteristics in single-crystal and polycrystalline TaN, Appl. Phys. Lett. 81 (2002) 1453–1455.

[31] C. Lee, Y.-L. Kuo, The evolution of diffusion barriers in copper metallization, JOM J. Miner. Met. Mater. S. 59 (2007) 44–49.

[32] L.E. Toth, Transition Metal Carbides and Nitrides, Academic Press, New York, 1971.

[33] J.-E. Sundgren, B.-O. Johansson, S.-E. Karlsson, H.T.G. Hentzell, Mechanisms of reactive sputtering of titanium nitride and titanium carbide II: Morphology and structure, Thin Solid Films. 105 (1983) 367–384.

[34] L. Hultman, J.-E. Sundgren, L.C. Markert, J.E. Greene, Ar and excess N incorporation in epitaxial TiN films grown by reactive bias sputtering in mixed Ar/N_2 and pure N_2 discharges, J. Vac. Sci. Technol. A . 7 (1989) 1187–1193.

[35] K.Y. Lim, Y.S. Lee, Y.D. Chung, I.W. Lyo, C.N. Whang, J.Y. Won, H.J. Kang, Grain boundary diffusion of Cu in TiN film by X-ray photoelectron spectroscopy, Appl. Phys. A Mater. 70 (2000) 431–434.